DOI: 10.13009/EUCASS2023-659
Aerospace Europe Conference 2023 – 10TH EUCASS – 9TH CEAS

Numerical simulation of the effect of different divergent angle of pylon

Prasanth P Nair†* and Vinod Narayanan**
** Mechanical Engineering Discipline, Indian Institute of Technology Gandhinagar, Gujarat, India, 382055*
prasanth.n@iitgn.ac.in – vinod@iitgn.ac.in
† Corresponding Author

Abstract
Scramjet engine is regarded as the future for reusable launch vehicles and high-speed transportation, nonetheless, the mixing and combustion of fuel present a difficulty at supersonic speeds. The supersonic velocity reduces the time available for the proper mixing of air and fuel. Researchers have noted that positioning a pylon before the cavity improves the efficiency of mixing. However, the impact of the pylon on the downstream region of the cavity remains unexplored. To address this gap, the current study investigates the consequences of fuel injection when a pylon is placed downstream of the cavity, exploring different divergent angles of the pylon to understand the impact of the pylon. Numerical simulation is employed, utilizing a hybrid RANS/LES simulation with an enhanced delayed detached eddy simulation (IDDES) turbulence model. The study reveals that the downstream placement of the pylon, in combination with different divergent angles, significantly influences the efficiency of mixing and the penetration height. To gain a deeper understanding of the mixing dynamics, additional investigation using dynamic mode decomposition (DMD) has been performed.

1. Introduction

Scramjet engines hold tremendous promise for the advancement of hypersonic flights. However, the design and optimization of these engines pose a multitude of challenges, particularly due to the unique operating conditions characterized by supersonic flow. A critical component of scramjet technology is the combustor, where the intricate process of fuel-air mixing takes place, resulting in combustion and the generation of propulsive thrust. The efficiency of this combustion process holds paramount importance in determining the overall performance of the engine.

To achieve optimal combustion, it is essential to enhance the mixing of fuel and air within the combustor while simultaneously maintaining a stable flame. Within the scope of scramjet combustors [1], researchers have primarily directed their attention toward two main types: strut-type [2–7] and cavity-type [8] combustors. The strut-type combustor incorporates a strategically positioned strut inside the combustion chamber to facilitate fuel injection into the airflow. This approach offers notable advantages concerning combustion stability and efficiency. However, it also introduces challenges associated with the interaction between the strut and the flowing airstream, resulting in the formation of complex vortical structures, intricate flow patterns, and increased total pressure loss.

Addressing these challenges, researchers have been actively exploring various strategies to design and optimize strut-type scramjet injectors. These strategies encompass a wide range of modifications, including alterations in the geometry and angle of the strut, as well as the implementation of different injection techniques, such as transverse and inclined injection. The current study focuses on cavity-based scramjet injection with a pylon. In cavity-based fuel injection, the fuel is injected within the cavity or upstream of the cavity, and the flame is stabilized through the cavity. In their comprehensive study, Ben-Yakar and Hanson [8] delve into the topic of cavity flame holders in the context of scramjets. The authors provide a detailed overview of cavity flame holders, shedding light on their diverse forms, including rectangular and trapezoidal shapes. By presenting a thorough examination of these variations, they offer valuable insights into their individual strengths and weaknesses. Wang et al. [9–11] conducted a series of experiments and numerical investigations to further explore the combustion dynamics within a cavity-based supersonic combustor. Their primary focus lies in investigating the effects of introducing hydrogen upstream of a cavity flame holder. They found that the combustion was stabilized by the localized flow condition around the shear layer. Expanding their investigations, Wang et al. [12] evaluated the performance of a dual-cavity scramjet combustor fueled by hydrogen. It

DOI: 10.13009/EUCASS2023-659

was found that the utilization of a dual-cavity design yields benefits, particularly in terms of improved mixing and enhanced combustion performance. Cavity-based axisymmetric scramjet model was researched by Liu et al. [13] operating at Mach 4.5. Their findings revealed that implementing a cavity flame holder resulted in notable enhancements in both the combustion efficiency and stability of the scramjet engine. Their study also indicated that the performance of flameholding was highly sensitive to both the geometry of the cavity and the configuration of fuel injection [14]. Roos et al. [15] conducted a computational analysis focusing on upstream crescent cavities in a scramjet combustor. Their study demonstrated that employing these upstream crescent cavities yielded superior combustion performance compared to conventional cavity-based combustors. Mecklem et al. [16] conducted numerical study on tandem cavities in an axisymmetric combustor. They found that tandem cavity pairs had improved combustion and heat release.
Moradi et al. [17] explored the influence of cavity shape on mixing efficiency in a supersonic flow. Their research revealed that a trapezoidal cavity flame holder exhibited the most optimal mixing characteristics. Gruber et al. [18] conducted an extensive investigation involving both numerical simulations and experimental studies on various cavity-based flame holders. Their results highlighted the effectiveness of cavity flame holders in stabilizing the flame under high-speed conditions, emphasizing that the choice of cavity geometry significantly impacted flameholding performance. Notably, the ramp angle of the cavity emerged as a crucial factor, with lower ramp angles resulting in shorter residence times. Edalatpour et al. [19] investigated the injection of multiple jets into a cavity-based flame holder. Their findings illustrated that an increase in momentum within the cavity contributed to improved mixing efficiency. Panigrahi et al. [20] explored the effects of a subcavity on oscillations within supersonic cavity flow, evaluating its potential to enhance or suppress such oscillations. Pudsey and Boyce [21] conducted numerical study on transverse jet through multiple ports. It was noted that the mixing performance was enhanced with small multiport injectors instead of injection through large injectors.

Karthick [22] conducted a study focusing on shock and shear layer interactions (SSLI) within a cavity-based flow, utilizing detached eddy simulation. The intensity of shock impingement was controlled by adjusting the ramp angle on the upper wall. The findings indicated that this approach, which coupled shock and oscillation cavity resonance, could serve as a passive flow control mechanism. Oamjee and Sadanandan [23] investigated the influence of various fuel injection angles and positions on mixing performance in a pylon-cavity flameholder. Their results revealed that altering the injection angle had a notable impact on both the height of fuel jet penetration, and the mixing efficiency. In a separate study, Li et al. [24] explored the potential for mixing enhancement through the use of an extended pylon in a cavity-based flameholder. Their research demonstrated that the introduction of an extended pylon positively influenced mixing. Verma and Vaidyanathan [25] conducted an experiment focused on the breakup and penetration of a liquid jet of acetone behind a pylon. They examined different flow rates and injection angles, observing a strong influence of the pylon on the jet breakup and penetration.

Recent investigations into cavity flameholders within supersonic flows have emphasized the significant role played by cavity geometry, injection configuration, and other design parameters in mixing efficiency and flameholding. However, prior studies did not consider the presence of a pylon downstream of the cavity. Therefore, the current numerical investigation addresses the impact of different angles of the pylon on the mixing performance within a configuration featuring a downstream pylon. Modal decomposition is employed as a mathematical tool to gain insights into the modes that contribute to the mixing performance.

2. Numerical methodology

The study employed computational analysis technique that focused on two-dimensional simulations. To accurately depict the intricate dynamics of turbulence, a hybrid approach combining Reynolds-Averaged Navier-Stokes (RANS) and Large Eddy Simulation (LES) was utilized. Specifically, an advanced variant known as improved delayed detached eddy simulation (IDDES) was employed, as it possesses the capability to effectively resolve turbulent vortices by adequately capturing the associated length scales [26–30]. In order to account for the complex behavior of turbulence in the near-wall region, the SST k-ω turbulence model was implemented as part of the RANS model. This model offers a more refined treatment of turbulence phenomena by taking into account the specifics of the near-wall flow behavior.

To validate the accuracy and reliability of the computational model, a flow solver in RANS mode was employed, similar to a previous study conducted by Karthick [22]. This approach served as a means of confirming the results obtained in the present research against the established findings of the earlier investigation. Additionally, the simulation encompassed the consideration of species transport, along with the inclusion of the ideal gas equation.

DOI: 10.13009/EUCASS2023-659

2.1 Geometry and grid details

The study employed a computational framework with the dimensions and geometry, as illustrated in Figure 1 (a), which was derived from an experimental investigation conducted by Gruber et al. [18]. For validation, a rectangular cavity was chosen for model validation, featuring a height (H) of 8.9 mm and a length of 3H. The computational domain extended 50H downstream of the cavity, and 10H upstream of the cavity with a height of the domain as 152 mm.

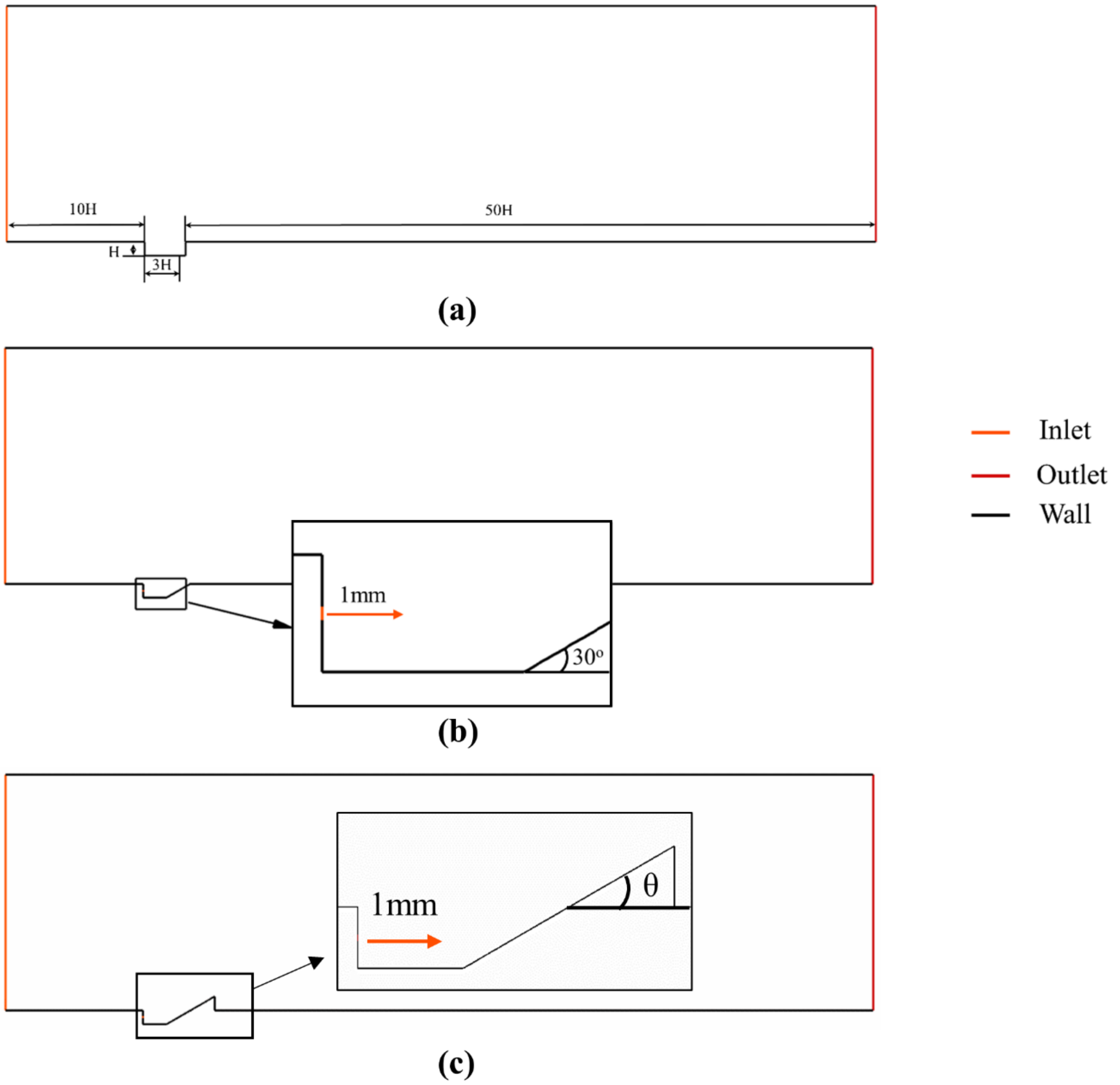

Figure 1: Computational domain with boundary definitions. (a) rectangular cavity used for validation, (b) base case, (c) different cases of the pylon downstream of the cavity

The computational domain had a similar extent as that of the validation case. The simulation has been compared with a base case, where the aft ramp angle was set at 30^{o}, as it was found to induce a more stable flow compared to smaller ramp angles, as shown in Figure 1 (b). The pylon was strategically positioned at the end of the cavity to introduce vortices downstream, and the angle of the pylon was varied to explore the impact of various diverging angles on the mixing performance, as depicted in Figure 1 (c).

The primary focus of the study was to analyze different cases of divergence of the pylon, aiming to assess both the effectiveness of the pylon downstream of the cavity and the implications of different divergent angles. A narrow slot of 1 mm width was utilized for hydrogen injection. Figure 1 (c) provides a visual representation of the angles of the pylon. To encompass a range of scenarios, four distinct configurations were examined having pylon divergence angles (θ) of 15^{o}, 30^{o}, 45^{o}, and 60^{o}, and these configurations were labeled as C15, C30, C45, and C60, respectively. To

DOI: 10.13009/EUCASS2023-659

facilitate a better understanding of the computational setup, Figure 1 also presents the boundary definitions employed in the simulations. The orange line denotes the inlet, the red line represents the outlet, and the black line signifies the walls enclosing the computational domain. Quadrilateral cells were produced for the simulation using ANSYS ICEM CFD. The mesh created in the hole and its immediate surroundings had an aspect ratio that varied from 1 to 1.95. A total of 517,579 quadrilateral cells were used for the validation. The mesh refinement was diligently performed to accurately capture vorticity and shock waves present in the study. The details of the grid independence study are provided in the previous study [30,31].

2.2 Boundary conditions and flow solver

The boundary conditions applied for the air and hydrogen at the inlet are presented in Table 1. The inflow pressure and temperature of air correspond to those utilized in a prior experimental investigation carried out by Gruber et al. [18]. The air is presumed to be vitiated air [32]. Regarding the wall, it is assumed to have a no-slip condition, which implies a velocity of zero at the wall. Furthermore, the wall is considered adiabatic.

Table 1: Air and hydrogen boundary conditions for the simulation

	Air	**Hydrogen**
T (K)	300	300
P (Pa)	690,000	690,000
Ma	3.0	1.0
Y_{O2}	0.232	0
Y_{N2}	0.736	0
Y_{H2O}	0.032	0
Y_{H2}	0	1

In order to enhance the accuracy of the numerical simulation, a double precision density-based coupled approach was employed, along with the AUSM flux splitting method. To minimize numerical errors, a second-order upwind scheme was utilized for spatial discretization. In terms of temporal discretization, a fourth-order R-K explicit time-stepping method was chosen due to its accuracy and stability. The time step was varied from 5e-8 to 1e-8 seconds to stabilize the numerical computation, and data were exported every 1e-6 seconds. For the dynamic mode decomposition (DMD) and time averaging, 1000 data files were saved. The DMD analysis was able to discern the spatiotemporal dynamics of the flow and gain a comprehensive understanding of the mechanisms involved in mixing.

3. Results and discussion

The validation and accuracy of the numerical model were verified by comparing it with the experimental data obtained from the work of Gruber et al. [18]. In a previous study [30,31], the numerical simulation, was validated both quantitively and qualitatively. The pressure profile, and schlieren images of the experiment matched with the numerical simulated result.

3.1 Flow features

Figure 2 shows the contour of the magnitude of the instantaneous density gradient. In the baseline case, a smooth transition of the flow is observed from the cavity to the downstream region when fuel is injected into the cavity. However, in all three injection cases with a downstream pylon, a highly turbulent and intricate flow is evident within the cavity, and downstream. The presence of the pylon obstructs the flow, leading to separation and reattachment, resulting in a sequence of vortices downstream of the pylon. The numerical investigation also detected weak shocks originating from the front and rear ends of the cavity during cavity injection, with their intersection occurring at a

DOI: 10.13009/EUCASS2023-659

certain distance. The acoustic waves have been clearly captured by the numerical simulation downstream of the pylon. As the diverging angle of the pylon increases, strong shocks are seen originating from the pylon that leads to flow separation ahead of the cavity, as seen in Figure 2(e).

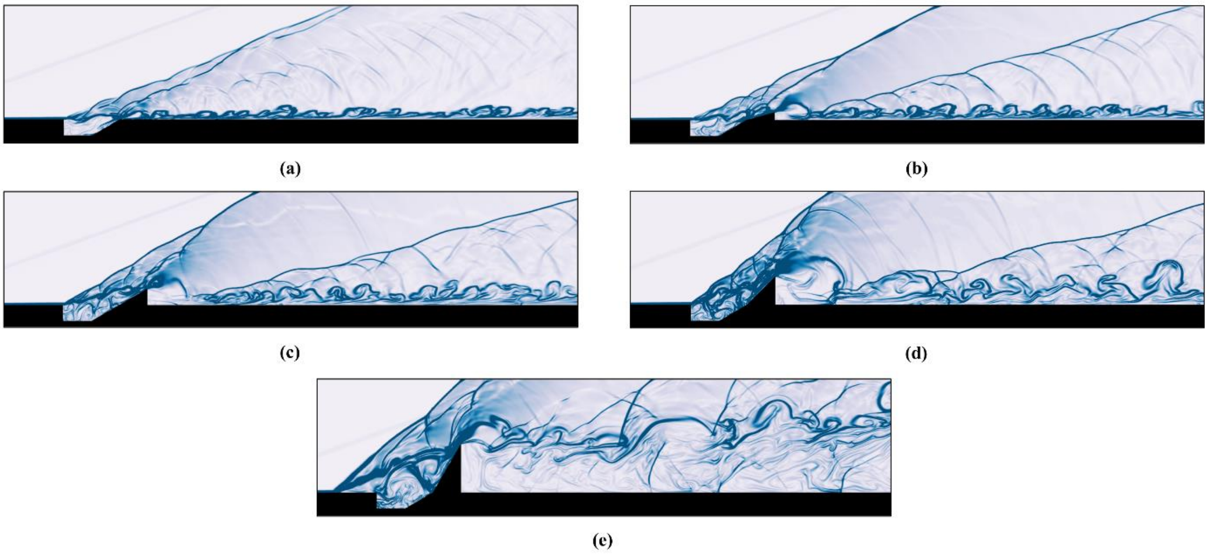

Figure 2: Instantaneous density gradient contour. (a) Base, (b) C15, (c) C30, (d) C45, and (e) C60

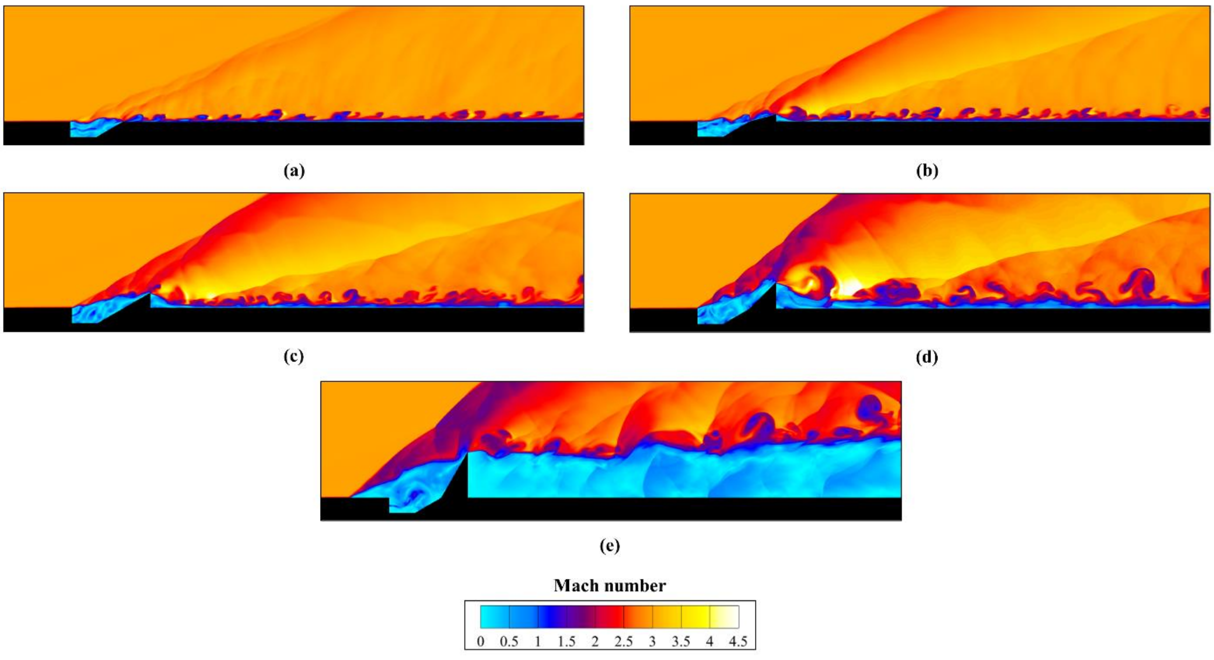

Figure 3: Instantaneous Mach number contour. (a) Base, (b) C15, (c) C30, (d) C45, and (e) C60

Cavity without pylon doesn't have a significant effect on the Mach number of the main flow. However, with the introduction of the pylon, strong oblique shocks and an expansion fan were observed. It was noted that with the increase in the angle of the pylon, the flow became subsonic downstream of the pylon, as seen in Figure 3. The C60 configuration had the highest extent of the subsonic region downstream of the pylon, with the wake region being completely subsonic, as observed in Figure 3 (e). Localized regions were found to have Mach number above 4, where an expansion region is formed downstream of the pylon (Figure 3 (c) and (d)).

DOI: 10.13009/EUCASS2023-659

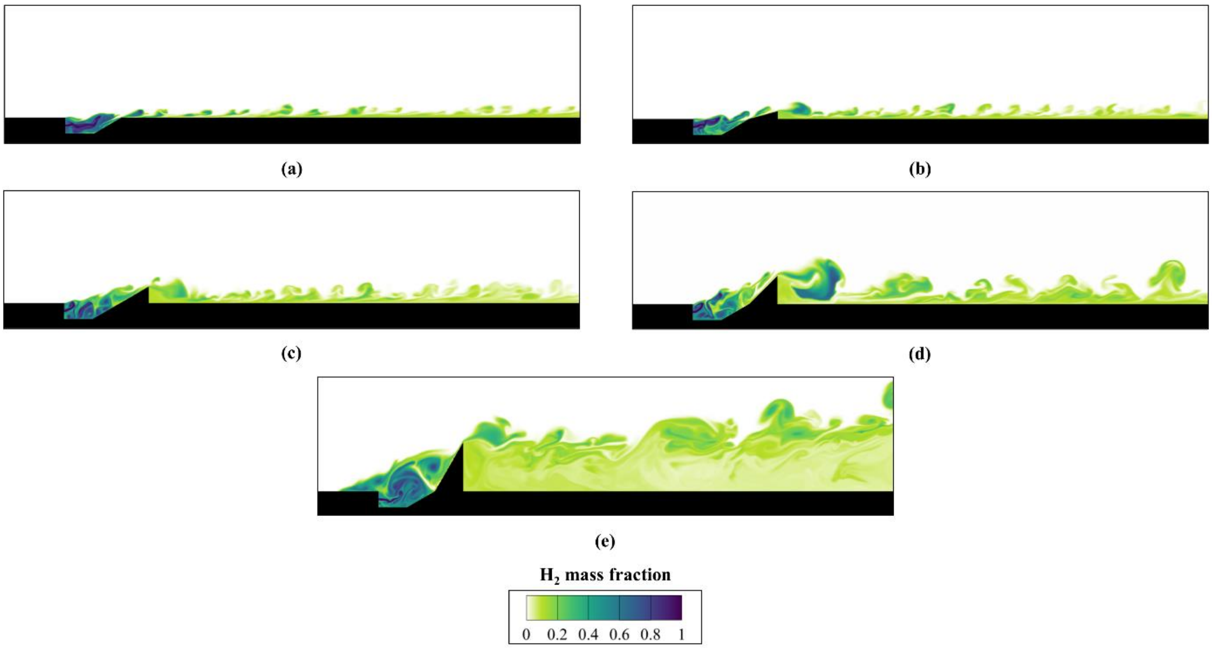

Figure 4: Instantaneous H_2 contour. (a) Base, (b) C15, (c) C30, (d) C45, and (e) C60

Figure 4 presents the contour plot of the hydrogen mass fraction at an instant. In the absence of a pylon for the base case, the hydrogen primarily accumulates within the cavity. As the cavity fills with hydrogen, it overflows, resulting in downstream mixing with the support of the wall. Conversely, the introduction of a pylon downstream of the cavity leads to the mixing of the hydrogen mass fraction with the incoming air due to the wake created by the pylon. This mixing phenomenon occurs in the wake of the pylon as the hydrogen flows over it. This observation suggests that the presence of a pylon modifies the flow pattern of hydrogen and enhances its mixing with the surrounding air. As depicted in Figure 4, with the increase in the angle of the pylon, the penetration height of the hydrogen fuel has also increased. The subsonic region created in the wake of the C60 configuration paves a path for the ideal mixing zone, however, this also restricts the air in the freestream to interact with the mixing zone due to momentum difference. The K-H instability assists in the mixing at the shear layer as the hydrogen flows over the pylon for the C60 configuration.

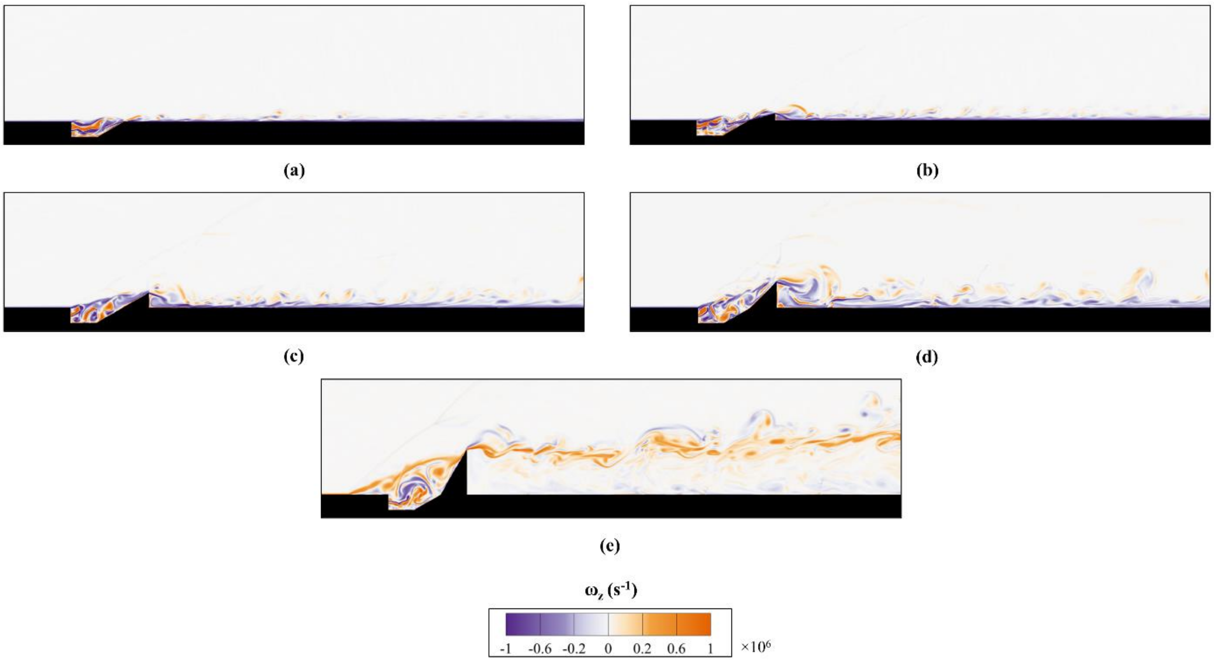

Figure 5: Instantaneous z-vorticity contour. (a) Base, (b) C15, (c) C30, (d) C45, and (e) C60

DOI: 10.13009/EUCASS2023-659

The instantaneous z- vorticity (ω_z) contour is shown in Figure 5. The figure illustrates that the configuration incorporating a pylon exhibits more pronounced and concentrated vortical structures within the cavity area, and downstream characterized by both clockwise and counter-clockwise rotations. In contrast, the configuration without the pylon displays comparatively weaker vortical structures, especially downstream of the pylon, as observed in Figure 5 (a). Furthermore, the wake region downstream of the cavity shows larger vortices when the pylon is present, indicating that the pylon has a notable influence on the formation and dynamics of vortices in the flow field. These observations strongly suggest that the presence of the pylon significantly impacts the flow physics, potentially altering the mixing and turbulence of the system. As the angle of the pylon increases, the size of the vortices are also observed to increase. In the case of the C60 configuration, vortices are observed primarily due to the K-H instability at the shear layer at the wake of the pylon.

3.2 Mixing efficiency and penetration height

The comparison of mixing efficiency and penetration height of all the configurations are shown in Figure 6. The mixing efficiency (η_m) is calculated quantitively using the expression below:

$$\eta_m = \frac{\int Y_f \, \rho u dA}{\int Y \, \rho u dA} \tag{1}$$

where

$$Y_f = \begin{cases} Y, & Y \le Y_s \\ Y_S(1 - Y)/(1 - Y_s), & Y > Y_S \end{cases} \tag{2}$$

where 0.0292 is the stoichiometric mass fraction of hydrogen (Y_s), and Y is the mass fraction of H_2.

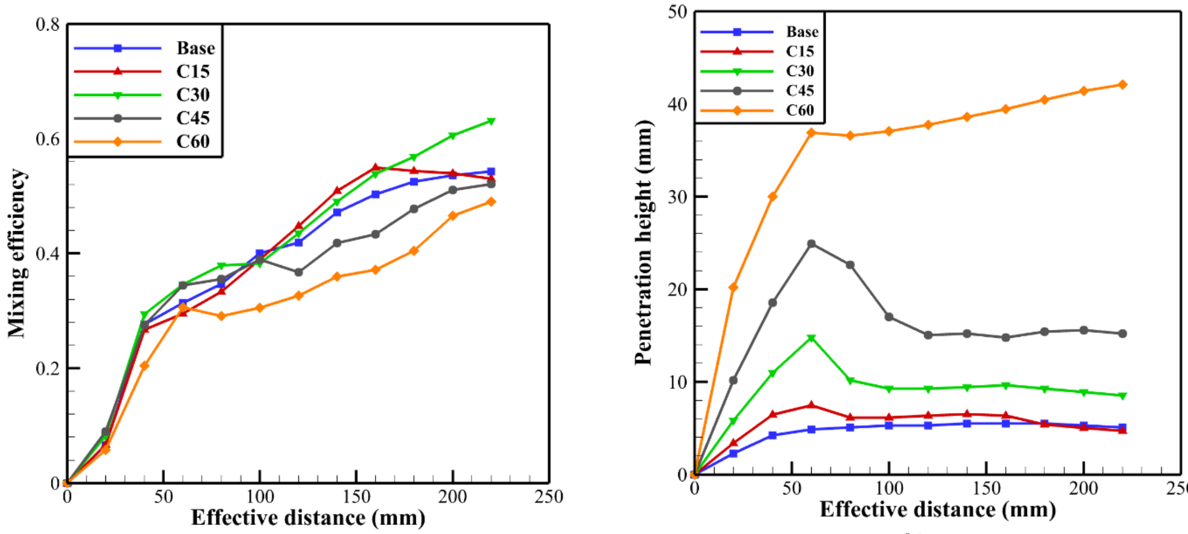

(a) (b)

Figure 6: Mixing efficiency and penetration height of different cases.

Figure 6 (a) shows the mixing efficiency of different configurations. The effective distance is the measurement that was initiated from the leading edge of the cavity. The data were taken with intervals of 20 mm. From the mixing efficiency plot, it is evident that the C30 configuration outperforms all the configuration and also serve as an optimal configuration. C15 configuration has better mixing efficiency until 160 mm. The decline might be caused due to the decreased penetration height after 160 mm, as observed in Figure 6 (b). It may be noted that both mixing efficiency and penetration height are important parameters [21]. The C60 case has the highest penetration height, however, it has the lowest mixing efficiency. As noted before, the majority of mixing in the case of C60 is due to K-H instability, while the wake region has minimal access to air for enhancement of mixing in the subsonic region. The C45 configuration had the second highest penetration height and, similarly, the second least mixing efficiency. It can be concluded that further optimization of the configuration could lead to a better mixing efficiency and penetration height.

DOI: 10.13009/EUCASS2023-659

3.3 DMD analysis of vorticity magnitude

Dynamic Mode Decomposition (DMD) is a data-driven technique employed to identify the dominant temporal modes [33–36]. In the context of determining mixing, vorticity plays a crucial role. Hence, the vorticity magnitude is subjected to DMD analysis. Figure 7 illustrates the DMD spectrum of the vorticity magnitude. The mode of zero frequency represents the mean mode. To normalize the amplitudes, they are scaled by the highest amplitude in the spectrum of DMD. The DMD spectrum reveals the dominant frequency of 19.32 kHz for the base configuration. The time dominant for C15, C30, C45, and C60 are 8.68 kHz, 5.7 kHz, 6.18 kHz, and 8.98 kHz, respectively. Implementation of the pylon is observed to bring down the dominating frequency of the DMD modes. It can also be noted that the C30 configuration has the lowest dominating frequency mode.

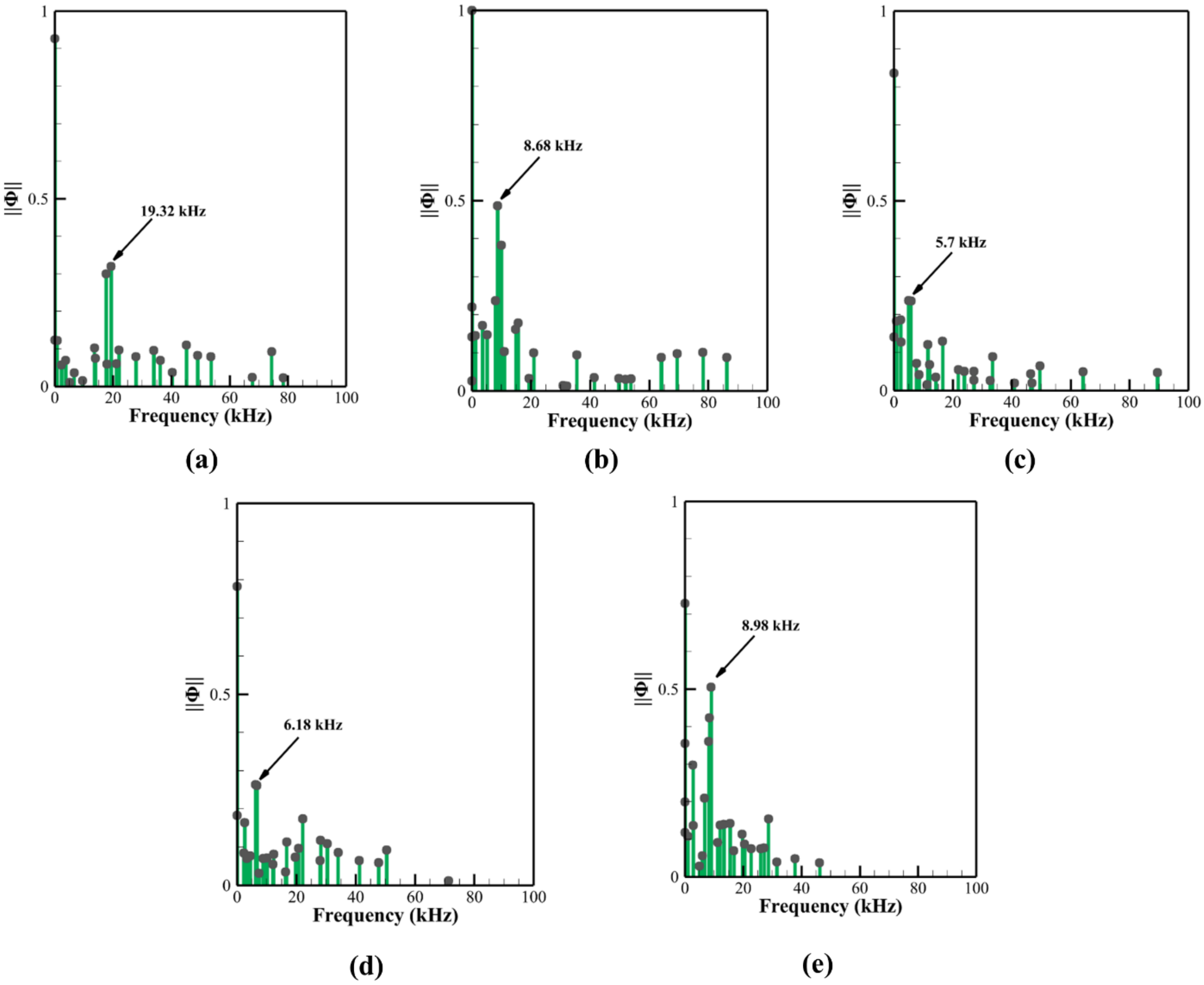

Figure 7: DMD spectrum of vorticity magnitude. (a) Base, (b) C15, (c) C30, (d) C45, and (e) C60

DOI: 10.13009/EUCASS2023-659

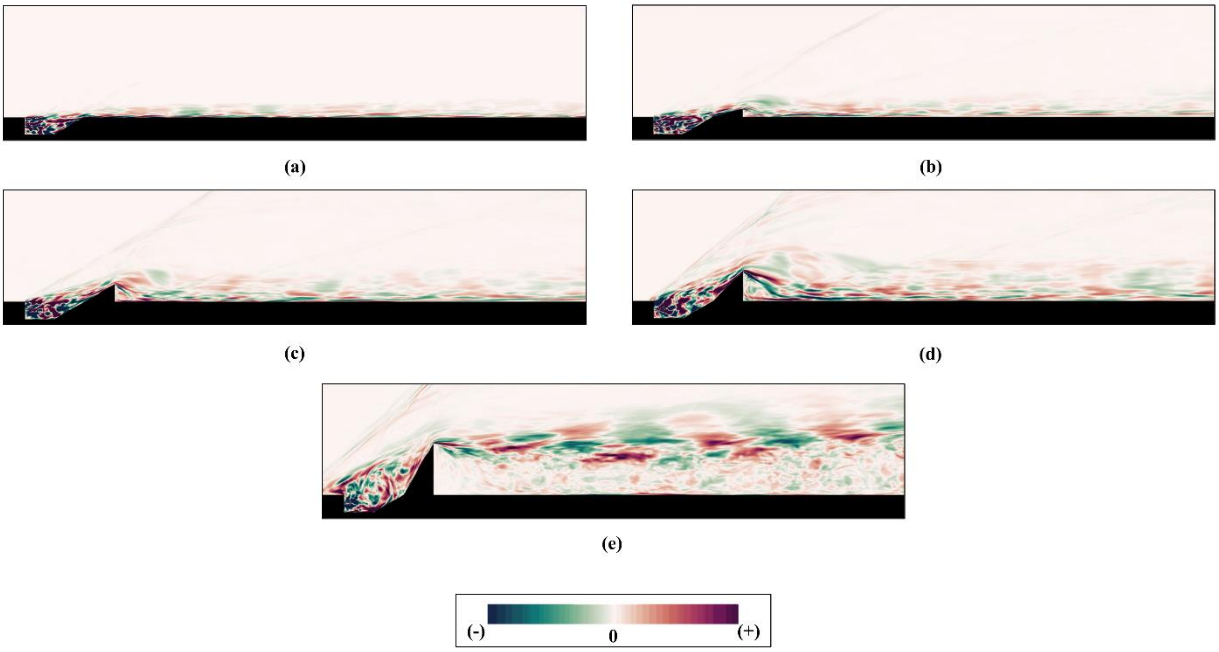

Figure 8: Contour of DMD mode of vorticity magnitude. (a) Base (19.32 kHz), (b) C15 (8.68 kHz), (c) C30 (5.7 kHz), (d) C45 (6.18 kHz), and (e) C60 (8.98 kHz)

The contour plot of the dominant modes identified using Dynamic Mode Decomposition (DMD), as depicted in Figure 7, are presented in Figure 8. In the base case, the dominant mode corresponds to the vorticity pattern within the cavity, which played a crucial role in enhancing the mixing efficiency, specifically within the cavity region. In the C15 and C30 cases, the coherent structures observed in the contour plot are primarily located within the cavity. These structures have a noticeable impact on the downstream vortices as well. These lower frequency modes contribute significantly to the mixing both within the cavity and in the downstream region. For the C45 case, a similar low frequency dominant mode is observed. This mode exhibits a similar effect on the flow dynamics, aiding in mixing within and immediately downstream of the cavity and pylon. The C60 case demonstrates a distinct mode that is responsible for mixing within the cavity and at the shear layer downstream of the pylon due to K-H instability. However, coherent structures within the wake region of the pylon of the C60 case are not prominent, hence leading to decreased mixing efficiency. These findings highlight the significance of different dominant modes in shaping the flow dynamics and enhancing mixing efficiency within and downstream of the pylon.

3. Conclusion

The study aimed to investigate the effects of different divergent angles of pylon downstream of the cavity on flow structure and mixing performance. To accurately capture the complex flow phenomena, an Improved Delayed Detached Eddy Simulation (IDDES) turbulence model was utilized. This model combines the strengths of both Reynolds-averaged Navier-Stokes (RANS) and large eddy simulation (LES) methods, providing a comprehensive understanding of the flow dynamics. To simplify the analysis and focus on the key aspects, the simulation was conducted in two-dimensional.

The results of the study revealed the significant impact of the pylon placement on the mixing performance and flow structure. The placement of the pylon downstream of the cavity created a blockage, causing the flow to undergo separation from and reattachment to the surface. This flow behavior resulted in the formation of a series of vortices downstream of the pylon. The interaction between these vortices and the flow within the cavity led to an enhanced mixing effect both within the cavity itself and in the downstream region. The pylon also assisted in increasing the penetration height.

To delve deeper into the underlying mechanisms responsible for this mixing enhancement, Dynamic Mode Decomposition (DMD) analysis was employed. The DMD analysis highlighted the importance of low-frequency vortices within the cavity and their interaction with the flow downstream of the pylon. These vortices created dynamic flow patterns that improved the overall mixing efficiency of the system.

DOI: 10.13009/EUCASS2023-659

References

[1] Liu, Q., Baccarella, D., and Lee, T. 2020. Review of Combustion Stabilization for Hypersonic Airbreathing Propulsion. *Prog. Aerosp. Sci.*, 119:100636. https://doi.org/10.1016/j.paerosci.2020.100636.

[2] Oevermann, M. 2000. Numerical Investigation of Turbulent Hydrogen Combustion in a SCRAMJET Using Flamelet Modeling. *Aerosp. Sci. Technol.*, 4(7):463–480. https://doi.org/10.1016/S1270-9638(00)01070-1.

[3] Gerlinger, P., Stoll, P., Kindler, M., Schneider, F., and Aigner, M. 2008. Numerical Investigation of Mixing and Combustion Enhancement in Supersonic Combustors by Strut Induced Streamwise Vorticity. *Aerosp. Sci. Technol.*, 12(2):159–168. https://doi.org/10.1016/j.ast.2007.04.003.

[4] Kumaran, K., and Babu, V. 2009. Investigation of the Effect of Chemistry Models on the Numerical Predictions of the Supersonic Combustion of Hydrogen. *Combust. Flame*, 156(4):826–841. https://doi.org/10.1016/j.combustflame.2009.01.008.

[5] Chang, J., Zhang, J., Bao, W., and Yu, D. 2018. Research Progress on Strut-Equipped Supersonic Combustors for Scramjet Application. *Prog. Aerosp. Sci.*, 103:1–30. https://doi.org/10.1016/j.paerosci.2018.10.002.

[6] Nair, P. P., S, A., Suryan, A., and Nizetic, S. 2021. Investigation of Flow Characteristics in Supersonic Combustion Ramjet Combustor toward Improvement of Combustion Efficiency. *Int. J. Energy Res.*, 45(1):231–253. https://doi.org/10.1002/er.5257.

[7] Nair, P. P., Narayanan, V., and Suryan, A. 2021. Combustion Efficiency Improvement for Scramjet Combustor with Strut Based Flame Stabilizer Using Passive Techniques. *Int. J. Hydrog. Energy*, 46(80):40054–40072. https://doi.org/10.1016/j.ijhydene.2021.09.224.

[8] Ben-Yakar, A., and Hanson, R. K. 2001. Cavity Flame-Holders for Ignition and Flame Stabilization in Scramjets: An Overview. *J. Propuls. Power*, 17(4):869–877. https://doi.org/10.2514/2.5818.

[9] Wang, H., Wang, Z., Sun, M., and Qin, N. 2013. Combustion Characteristics in a Supersonic Combustor with Hydrogen Injection Upstream of Cavity Flameholder. *Proc. Combust. Inst.*, 34(2):2073–2082. https://doi.org/10.1016/j.proci.2012.06.049.

[10] Wang, H., Wang, Z., and Sun, M. 2013. Experimental Study of Oscillations in a Scramjet Combustor with Cavity Flameholders. *Exp. Therm. Fluid Sci.*, 45:259–263. https://doi.org/10.1016/j.expthermflusci.2012.10.013.

[11] Wang, H., Wang, Z., Sun, M., and Qin, N. 2013. Large-Eddy/Reynolds-Averaged Navier–Stokes Simulation of Combustion Oscillations in a Cavity-Based Supersonic Combustor. *Int. J. Hydrog. Energy*, 38(14):5918–5927. https://doi.org/10.1016/j.ijhydene.2013.02.100.

[12] Wang, H., Wang, Z., Sun, M., and Qin, N. 2015. Large Eddy Simulation of a Hydrogen-Fueled Scramjet Combustor with Dual Cavity. *Acta Astronaut.*, 108:119–128. https://doi.org/10.1016/j.actaastro.2014.12.008.

[13] Liu, Q., Baccarella, D., McGann, B., and Lee, T. 2019. Cavity-Enhanced Combustion Stability in an Axisymmetric Scramjet Model. *AIAA J.*, 57(9):3898–3909. https://doi.org/10.2514/1.J058204.

[14] Liu, Q., Baccarella, D., Landsberg, W., Veeraragavan, A., and Lee, T. 2019. Cavity Flameholding in an Optical Axisymmetric Scramjet in Mach 4.5 Flows. *Proc. Combust. Inst.*, 37(3):3733–3740. https://doi.org/10.1016/j.proci.2018.08.037.

[15] Roos, T., Pudsey, A., and Ogawa, H. 2021. Numerical Investigation of Combustion Characteristics of Upstream Crescent Cavities in a Scramjet Combustor. *Acta Astronaut.*, 187:43–60. https://doi.org/10.1016/j.actaastro.2021.05.027.

[16] Mecklem, S. A., Landsberg, W. O., Curran, D., and Veeraragavan, A. 2022. Combustion Enhancement via Tandem Cavities within a Mach 8 Scramjet Combustor. *Aerosp. Sci. Technol.*, 124:107551. https://doi.org/10.1016/j.ast.2022.107551.

[17] Moradi, R., Mahyari, A., Barzegar Gerdroodbary, M., Abdollahi, A., and Amini, Y. 2018. Shape Effect of Cavity Flameholder on Mixing Zone of Hydrogen Jet at Supersonic Flow. *Int. J. Hydrog. Energy*, 43(33):16364–16372. https://doi.org/10.1016/j.ijhydene.2018.06.166.

[18] Gruber, M. R., Baurle, R. A., Mathur, T., and Hsu, K.-Y. 2001. Fundamental Studies of Cavity-Based Flameholder Concepts for Supersonic Combustors. *J. Propuls. Power*, 17(1):146–153. https://doi.org/10.2514/2.5720.

[19] Edalatpour, A., Hassanvand, A., Gerdroodbary, M. B., Moradi, R., and Amini, Y. 2019. Injection of Multi Hydrogen Jets within Cavity Flameholder at Supersonic Flow. *Int. J. Hydrog. Energy*, 44(26):13923–13931. https://doi.org/10.1016/j.ijhydene.2019.03.117.

[20] Panigrahi, C., Vaidyanathan, A., and Nair, M. T. 2019. Effects of Subcavity in Supersonic Cavity Flow. *Phys. Fluids*, 31(3):036101. https://doi.org/10.1063/1.5079707.

[21] Pudsey, A. S., and Boyce, R. R. 2010. Numerical Investigation of Transverse Jets Through Multiport Injector Arrays in a Supersonic Crossflow. *J. Propuls. Power*, 26(6):1225–1236. https://doi.org/10.2514/1.39603.

[22] Karthick, S. K. 2021. Shock and Shear Layer Interactions in a Confined Supersonic Cavity Flow. *Phys. Fluids*, 33(6):066102. https://doi.org/10.1063/5.0050822.

DOI: 10.13009/EUCASS2023-659

[23] Oamjee, A., and Sadanandan, R. 2020. Effects of Fuel Injection Angle on Mixing Performance of Scramjet Pylon-Cavity Flameholder. *Phys. Fluids*, 32(11):116108. https://doi.org/10.1063/5.0026125.

[24] Li, Z., Barzegar Gerdroodbary, M., Sheikholeslami, M., Shafee, A., Babazadeh, H., and Moradi, R. 2020. Mixing Enhancement of Multi Hydrogen Jets through the Cavity Flameholder with Extended Pylon. *Acta Astronaut.*, 175:300–307. https://doi.org/10.1016/j.actaastro.2020.06.002.

[25] Verma, N., and Vaidyanathan, A. 2020. Liquid Jet Breakup behind a Pylon in Supersonic Flow. *Exp. Therm. Fluid Sci.*, 113:109984. https://doi.org/10.1016/j.expthermflusci.2019.109984.

[26] Gritskevich, M. S., Garbaruk, A. V., Schütze, J., and Menter, F. R. 2012. Development of DDES and IDDES Formulations for the K-ω Shear Stress Transport Model. *Flow Turbul. Combust.*, 88(3):431–449. https://doi.org/10.1007/s10494-011-9378-4.

[27] Wang, H., Shan, F., Piao, Y., Hou, L., and Niu, J. 2015. IDDES Simulation of Hydrogen-Fueled Supersonic Combustion Using Flamelet Modeling. *Int. J. Hydrog. Energy*, 40(1):683–691. https://doi.org/10.1016/j.ijhydene.2014.10.124.

[28] Nair, P. P., Suryan, A., and Narayanan, V. 2022. Modal Analysis of Mixing Characteristics in Scramjet Combustor with Passive Struts. *Int. J. Hydrog. Energy*, 47(81):34656–34675. https://doi.org/10.1016/j.ijhydene.2022.08.061.

[29] Nair, P. P., and Narayanan, V. 2023. Numerical Study on the Effect of Equivalence Ratio in Passive Strut Configuration. In: *AIAA SCITECH 2023 Forum*, AIAA 2023-1645. https://doi.org/10.2514/6.2023-1645

[30] Nair, P. P., and Narayanan, V. 2023. Numerical Study on the Effect of the Pylon Downstream of the Cavity-Based Scramjet Combustor. In: *8th Thermal and Fluids Engineering Conference (TFEC)*, pp. 5-15. https://doi.org/10.1615/TFEC2023.aer.046452

[31] Nair, P. P., and Narayanan, V. 2023. Effect of Injection Method on the Pylon Placed Downstream of the Cavity. In: *AIAA AVIATION 2023 Forum*, AIAA 2023-4137, https://doi.org/10.2514/6.2023-4137.

[32] Génin, F., and Menon, S. 2010. Simulation of Turbulent Mixing Behind a Strut Injector in Supersonic Flow. *AIAA J.*, 48(3):526–539. https://doi.org/10.2514/1.43647.

[33] Schmid, P. J. 2010. Dynamic Mode Decomposition of Numerical and Experimental Data. *J. Fluid Mech.*, 656:5–28. https://doi.org/10.1017/S0022112010001217.

[34] Kutz, J. N., Brunton, S. L., Brunton, B. W., and Proctor, J. L. 2016. *Dynamic Mode Decomposition*. Society for Industrial and Applied Mathematics.

[35] Schmid, P. J. 2022. Dynamic Mode Decomposition and Its Variants. *Annu. Rev. Fluid Mech.*, 54(1):225–254. https://doi.org/10.1146/annurev-fluid-030121-015835.

[36] Nair, P. P., Suryan, A., and Narayanan, V. 2023. Effect of Passive Strut Angle on the Vortical Structures and Mixing Characteristics of Scramjet Combustor. *Phys. Fluids*, 35(6):066111. https://doi.org/10.1063/5.0151676.